The role of the number of filaments in the dissociation of CO 2 in dielectric barrier discharges

Claire Douat, Srinath Ponduri, T. Boumans, Olivier Guaitella, Stefan Welzel, Emile Carbone, Richard Engeln

Plasma Sources Science and Technology

PAPER • **OPEN ACCESS**

The role of the number of filaments in the dissociation of CO_2 in dielectric barrier discharges

To cite this article: C Douat *et al* 2023 *Plasma Sources Sci. Technol.* **32** 055001

OPEN ACCESS
IOP Publishing
Plasma Sources Science and Technology
Plasma Sources Sci. Technol. **32** (2023) 055001 (14pp)
https://doi.org/10.1088/1361-6595/acceca

The role of the number of filaments in the dissociation of CO_2 in dielectric barrier discharges

C Douat[1,2,*], S Ponduri[1], T Boumans[1], O Guaitella[3], S Welzel[1,4], E Carbone[5] and R Engeln[1,6]

[1] Eindhoven University of Technology, PO Box 513, 5600 MB, Eindhoven, The Netherlands
[2] GREMI, UMR 7344, CNRS/Université d'Orléans, BP, 6744, 45067 Orléans Cedex 2, France
[3] LPP, Ecole Polytechnique, UPMC, Université Paris Sud XI, CNRS, Palaiseau, France
[4] DIFFER—Dutch Institute for Fundamental Energy Research, Eindhoven, The Netherlands
[5] Institut National de la Recherche Scientifique, centre Energie, Matériaux et Télécommunications, 1650, blvd Lionel Boulet, J3X 1S2 Varennes, QC, Canada
[6] ASML, De Run 6501, 5504 DR Veldhoven, The Netherlands

E-mail: claire.douat@univ-orleans.fr

Received 28 November 2022, revised 3 April 2023
Accepted for publication 20 April 2023
Published 5 May 2023

Abstract

An experimental investigation of the dissociation of CO_2 in a symmetric pin-to-pin dielectric barrier discharge (DBD) is presented. The reactor geometry allows for an accurate control of the number of filaments (microdischarges) and is used to study the impact of one single filament on the CO_2 dissociation. We show the number of filaments per half cycle follows a power-law as a function of the injected power and does not depend on pressure, flow or other process parameters. It is shown that for pressures between 200 and 700 mbar approximately 0.5 W per filament is required and the charge transferred per filament remains constant at 0.5 nC. Furthermore, the dependence of CO_2 conversion on only specific energy input (SEI) is shown to be valid down to a single filament. Additionally, by using quantum cascade laser absorption spectroscopy the absolute number of CO molecules produced per filament is measured and is found to be in the range from 5.10^{11} to 2.10^{12}. The conversion degree of CO_2 into CO is estimated to be lower than 0.1% within a single filament and increases with SEI. In the presence of a couple of filaments, the maximum energy efficiency obtained is 25%. A comparison of the conversion degrees in pin-to-pin DBD and plane-to-plane DBD configuration shows that these two reactor geometries follow the same power law. This means the geometry is not the most important parameter in CO_2 dissociation in DBDs, but the SEI and thus the number of filaments ignited per unit of time. This result means that the dependence of conversion degree on the SEI can be extended to a single filament. This observation leads to the conclusion that the SEI appears to be valid as a universal scaling parameter down to very low values.

Keywords: CO_2 dissociation, DBD, absorption spectroscopy, QCL, solar fuels, filament

(Some figures may appear in colour only in the online journal)

* Author to whom any correspondence should be addressed.

1. Introduction

The study of the dissociation of CO_2 into CO by non-equilibrium plasma is a topic of great interest due to its importance in the energy storage field. The continued and projected increase use of fossil fuels, owing to its limited availability, presents a major energy supply and environmental problem. An alternative to this issue is the use of renewable energy. To counterbalance their intermittency, one possible solution is to store the excess energy in a chemical form by reforming CO_2 into fuel. The most energy consuming step of this process is the dissociation of CO_2 into CO. A promising route to achieve high CO_2 conversion, while keeping investment and running costs low, is probably to use plasma-assisted dissociation [1]. The key enabler for this is that non-thermal plasmas can utilize electricity generated by renewable energy for CO_2 conversion. In addition to being an important step in storage of renewable energy, plasma assisted CO_2 dissociation can be used in other applications. CO_2 dissociation leads the formation of CO, which is an important molecule in biology and shows therapeutic features in medicine [2, 3], while CO_2 dissociation could also be used to produce oxygen on Mars [4].

The dissociation of CO_2 has been explored in different plasma sources and under various discharge conditions, such as corona discharges [5], gliding arcs [6], microwave plasmas [7, 8] and dielectric barrier discharges (DBD) [9–16]. While all plasma sources have their benefits, DBDs are ideal for gas conversion as they can be sustained at low gas temperatures [17–19], while simultaneously producing significant quantities of reactive species [20]. Furthermore, to improve the efficiency in CO_2 conversion, DBDs can be used with a catalyst [21] which explains the popularity in using DBDs at industrial scales [22]. Also, DBDs are easy to realize with relatively cheap equipment and hence are used in benchmarking diagnostic techniques [23, 24]. In addition to purely using gas based DBDs which are the main topic of this paper, packed bed reactors are interesting, in that a catalyst can be introduced to exploit the synergistic effect between plasma and surface [25, 26]. However, packed bed reactors do not give optical access hence are not suitable for *in situ* studies of the fundamentals of gas phase chemistry.

Brehmer *et al*, made fundamental experimental studies on CO_2 dissociation in DBDs using a symmetric planar configuration [9, 24, 27]. In these works, the effect of various parameters such as the gap between the two electrodes, the gas flow rate, the repetition frequency of the applied voltage, and the thickness of the dielectric layers were studied in detail. They showed that the specific energy input (SEI), which represents the average amount of energy that is spent on each molecule of the gas, is a universal scaling parameter to determine the conversion degree, usually called α in the literature. No matter how a given specific energy is attained, using any combination of pressure, applied voltage, flow, frequency, gap, dielectric thickness, the conversion degree remains constant for that energy. They showed that the dependence between them is approximately a power law, where $\alpha = \text{Constant} \times \text{SEI}$, with $n \approx 0.75$. Later Aerts *et al* have reported similar scaling law with very low flows and different types of dielectric materials and achieved a higher degree of CO_2 conversion [28]. This scaling behavior has been explained by numerical models, and it predicts that dissociation is dominated by direct electron impact reactions [28, 29].

When operated in filamentary mode a DBD is characterized by plasma channels called filaments or micro-discharges that are spread stochastically over space and in time [30]. In this mode the superposition of multiple micro-discharges makes it complicated to study the impact of one single filament on CO_2 dissociation. Most of the works on CO_2 dissociation with DBD in pure CO_2 were performed in regimes where several filaments occur, making their number complicated to measure [9–16]. As explained by Brandenburg, micro-discharge is the most fundamental element of a filamentary DBD and its optimization is important for the development of applications [31]. Höft *et al* showed that in N_2 DBD, with a small admixture of O_2, most of the results obtained for single-filament DBDs can be directly transferred to multi-filament arrangements [32]. In pure CO_2 DBD it was not reported that the power law described above for multi-filaments is transferrable to single-filament.

In order to fill this gap a DBD reactor in pin-to-pin configuration has been built. This configuration is chosen to confine the filament(s) to a known location and have control over the temporal evolution. The geometry restricts the available space for a filament to occur thus reducing the number of filaments and ensuring that each independent filament can still be resolved either by electrical characterization, optical characterization or both. The strategy to isolate single filaments and study the fundamental aspects of a DBD is widely used [32, 33].

Infrared absorption spectroscopy with a quantum cascade laser (QCL) was used to correlate CO produced by a single filament. The CO density was measured in the exhaust similar to Brehmer *et al* [9], and an estimation of the absolute number of CO molecules per filament is established which can be used to benchmark the numerical models such as Eliasson *et al* [17], Ponduri *et al* [34] etc. Moreover, energy efficiency for CO generation is estimated for a single filament.

2. Experimental setup

2.1. Plasma reactor

The reactor geometry and the experimental setup for measuring the CO density are shown schematically in figure 1. The experiments are carried out in a setup consisting of two tungsten electrodes covered with soda-lime silica glass. The two electrodes are placed opposite to each other in pin-to-pin configuration. The dimensions and electrical parameters of the reactor are presented in table 1. The plasma is powered with a sinusoidal high voltage (10–25 kV peak to peak) at 22 kHz using an AC generator (AMPTEC). The electrodes are mounted inside a cylindrical glass cell connected to a vacuum pump to maintain reproducible gas conditions. The cylindrical

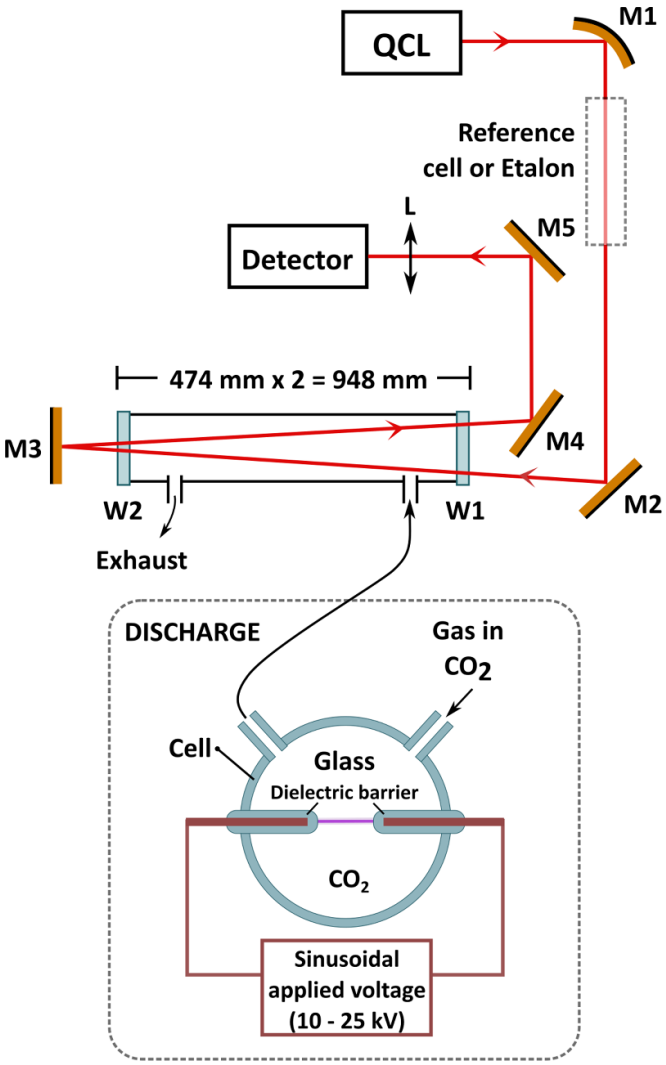

Figure 1. Diagnostic technique applied to measure the CO density *ex situ*. The discharge is created in pure CO_2 gas inside a cylindrical glass cell connected to a vacuum pump to maintain reproducible gas conditions. The cell consists of two tungsten electrodes covered with soda-lime silica glass with 1.7 mm gap. The CO density in the effluent of the DBD is measured by an *ex-situ* IR absorption spectroscopy method with a QCL with a double-pass cell composed by a stainless-steel tube of length 474 mm and two KBr windows (IR transparent material).

geometry of the cell assures good gas recirculation. A gas flow rate of 100–700 standard cubic cm per minute (sccm) is used. The pressure in the cell is between 400 and 700 mbar which is established using a rotary pump at the exhaust. The experiments are performed in CO_2 with 99.9% purity (Linde, 4L food-grade).

During all experiments, no carbon deposits have been observed on the surface of the DBD or on the cell windows, even after several hours of operation. The absence of deposits may be correlated with the relatively low conversion rates in the present study as compared to Belov *et al* where such observation was made [15].

Table 1. Dimensions and electrical parameters of the plasma reactor used in this work.

Parameters	Reactor
Electrodes gap (*D*)	1.7 mm
Inner volume of the cell	65 cm^3
Diameter electrode (*d*)	1.0 mm
Thickness glass layer (*e*)	1 mm
Resonance frequency (*f*)	22 kHz
Volume of the active discharge zone	19 mm^3

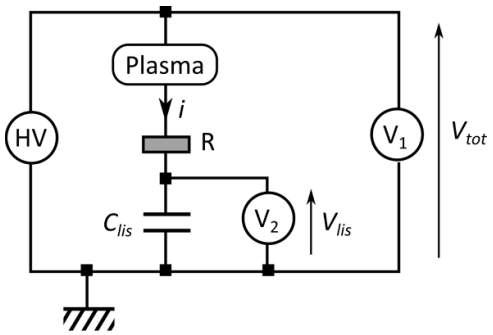

Figure 2. Schematic drawing of the electronic circuit employed to operate the DBD reactor with accessories for electrical characterization. The voltage signal applied to the reactor (V_1) is measured by means of a Tektronix probe (P6015A with 1000:1 division ratio), while the current is measured with a Rogowski coil (Pearson current monitor 4100) placed in series with the DBD (R). Transferred charges are collected on a capacitor (C_{lis} = 140 pF) to obtain the power absorbed by the plasma via the Lissajous method, and are detected using a commercial voltage probe, V_2 (Rigol, RP3300, 1001).

2.2. Electrical characterization

A fast digitizing oscilloscope (LeCroy Waverunner 610zi, 1 GHz) is used to perform electrical measurements. Figure 2 shows a schematic drawing of the electric circuit. The voltage signal applied to the reactor (V_1) is measured by means of a Tektronix probe (P6015A with 1000:1 division ratio), while the current is measured with a Rogowski coil (Pearson current monitor 4100). The latter is placed in series with the DBD (R). We choose as repetition frequency of the applied voltage, the one corresponding to the resonance frequency, *f*, of the total circuit in order to limit heating of the power supply and maximize power transfer efficiency to the plasma. The driving frequency is 22 kHz, and has been determined experimentally. Figure 3 shows typical *I*–*V* characteristics.

Transferred charges are collected on a capacitor (C_{lis} = 140 pF) to obtain the power absorbed by the plasma via the Lissajous method, and are detected using a commercial voltage probe, V_2 (Rigol, RP3300, 100:1) [35, 36]. The area of the curve formed by the transferred charges, *Q*, as a function of the applied voltage, V_{tot}, is proportional to the injected energy per AC cycle, E_{cycle}, and thus to the power input (i.e. the power absorbed by the plasma) $P_{In} = fE_{cycle}$ where *f* is the driving frequency. Two examples of *Q*–*V* plot

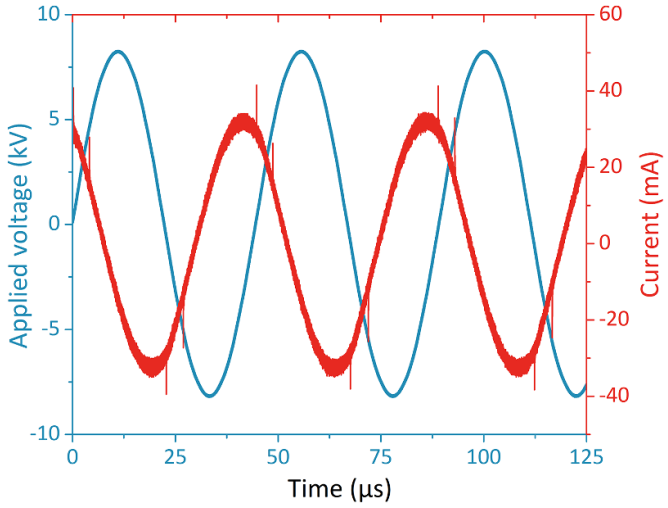

Figure 3. Current voltage characteristics at 700 mbar, 700 sccm CO_2 flow and 17 kV peak-to-peak applied voltage.

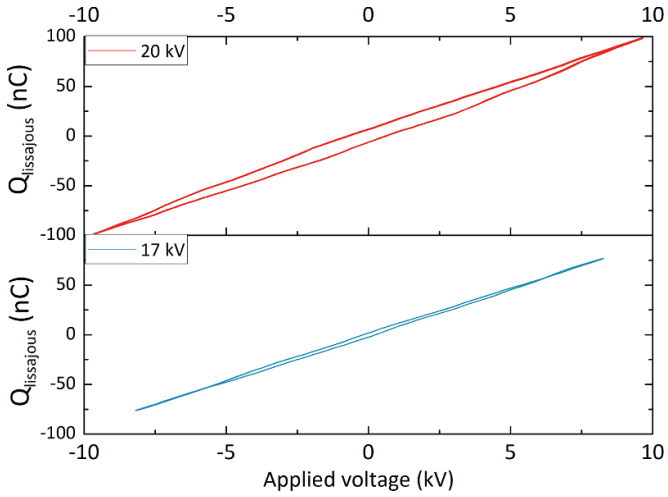

Figure 4. Q–V plots showing the transferred charges through the reactor as a function of the applied voltage under two different applied voltages. The area of the Q–V plot is used to determine the energy injected per cycle to the plasma. Conditions: 700 mbar, 700 sccm CO_2.

are shown in figure 4. The area of the loop increases with the applied voltage, and for low voltages the measure of the area is therefore not very accurate and it is accounted by bigger error margins.

The average number of filaments per half-cycle, N_{avg}, is counted using the waveforms from the current probe. For example, in figure 3, there are two current spikes per half cycle, which means two filaments are produced. Number of filaments per half cycle was determined by measuring current for 50–60 cycles. Measuring such large number of cycles enables to get good statistics on filament distribution. It is interesting to notice that the positive and the negative parts of the current waveform are symmetrical. This is due to the fact that the two electrodes are identical and both are covered with a dielectric layer [15]. As no change of the current waveform is observed

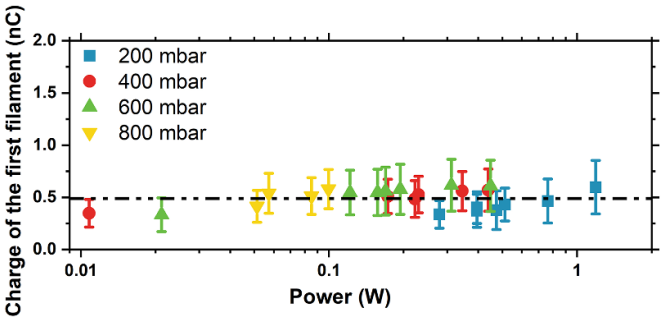

Figure 5. Charge transferred in the first filament at various gas pressures: 200 mbar (blue square), 400 mbar (red circle), 600 mbar (green up-pointing triangles) and 800 mbar (yellow down-pointing triangles). The dashed line at 0.5 nC is to accentuate the fact that the charge transferred in the first filament is approximately constant across the pressure and power range.

in time, it supports the fact that there is no carbon deposition in the present reactor. Carbon deposition would induce a change on the conductivity of the electrodes, and therefore would imply a modification of the electrical signal [15].

In specific conditions, two filaments can occur simultaneously and provide one current spike. Usually, this happens in pulse excitation, when an over-voltage breakdown occurs [37, 38]. For sufficiently fast-applied voltage rise times, the voltage at breakdown can exceed the static breakdown voltage, which results in a higher initial electric field upon breakdown [38]. Thus, this intense electric field can ignite more filaments simultaneously. In AC operation, breakdown occurs when the voltage across the discharge gap reaches a value, which is essentially the static breakdown voltage [38]. Due to the slow rise of the AC waveform, the probability to ignite more than one filament per current spike is low. As we used an AC excitation and from the intensified charge-coupled device (iCCD acquisition), we only observed one filament per current spike, we can reasonably assume that each current spike represents one filament.

The average charge transferred by the first filament alone in a half cycle is measured by measuring the change in the Lissajous capacitor voltage when the filament occurs ($q = C_{lis} \times V_{lis}$) and is plotted in the figure 5. By taking into account the error bars (the error bars represent the standard deviation of a data set), the charge remains constant at 0.5 nC irrespective of pressure, which is in good agreement with Eliasson *et al*, who showed that the charge transferred per filament should be constant at all pressures [39]. This result ensures that only one filament occurs at each current spike, otherwise the charge transferred by a filament would be twice as large.

Fast optical imaging is used to capture the light emission from the first and the second filament. Due to the jitter, the third and subsequent filaments cannot be measured with a good accuracy. As the light emission from individual filaments in CO_2 DBD is very weak, single shot measurements of one single filament are too noisy. To overcome this issue, the measurements are accumulated to increase the signal to noise ratio. To ensure that the light is collected from only one

current spike, the camera is gated. The pictures support the interpretation that the first current peak corresponds to a single filament located in the region with the shortest gap and the second current peak corresponds to a filament randomly distributed around this region. The latter forms when the voltage reaches sufficient values for generating a second avalanche in a region where the applied electric field is not shielded by deposited charges on the dielectric.

In order to compare the present experimental results directly with other works on CO_2 dissociation, different parameters, such as the SEI, the conversion degree and the energy efficiency are used here. According to the previous works related to CO_2 dissociation into CO, the SEI can be considered as the universal parameter for comparisons between plasma sources [9, 12, 29, 34, 40–42]. The latter, denoted as E_{spec} or SEI, represents the average amount of energy that is spent on each molecule injected into the reactor without taking into account if dissociation of the molecule has occurred or not. This parameter is defined as

$$E_{spec}\,(J/l) = \mathrm{SEI} = \frac{P_{In}\,(W)}{\varphi\,(l/s)} \tag{1}$$

where P_{In} is the power input and φ the total gas flow rate. Note that the latter is expressed in standard conditions ($T_0 = 273.15$ K, $p_0 = 1013.25$ mbar). The parameter which defines the amount of CO_2 dissociated into CO is the conversion degree. This is the ratio of the final CO density over the total gas density, n, equivalent to the CO_2 density,

$$\alpha_{abs} = \frac{[CO]_{final}}{[CO_2]_{inital}} = \frac{[CO]_{final}}{n}. \tag{2}$$

The final CO density, $[CO]_{final}$, is measured by means of absorption spectroscopy and the technique is explained in the following section, while the initial CO_2 density,$[CO_2]_{initial}$ is calculated from the input parameters such as the pressure and the gas flow rates.

While the conversion degree gives an information on the amount of CO molecule created, to make CO from renewable energy source it is also important to measure the fraction of energy used for this conversion. The energy efficiency, η, reflects this aspect, and throughout this paper will be expressed as

$$\eta = \frac{\Delta H}{E_{spec}} \cdot \alpha \tag{3}$$

where ΔH is the enthalpy of formation of CO from CO_2 taken at room temperature (i.e. the amount of energy stored chemically into CO that can be recovered by oxidizing it) and the conversion process can be summarized as

$$CO_2 \rightarrow CO + {}^1\!/_2\, O_2.\ \Delta H = 2.9\ \mathrm{eV} \tag{R1}$$

η gives a measure of how efficient a plasma source is in utilizing the electrical energy for CO_2 conversion and no other process such as heating the gas etc.

2.3. Laser absorption system and data analysis

The CO density in the effluent of the DBD is measured by an *ex-situ* IR absorption spectroscopy method with a quantum cascade laser (QCL). The diagnostic setup with the implementation of the DBD is shown in figure 1. The latter is similar to the one used Douat *et al* [43], except that the multi-pass cell is replaced by a double-pass cell. The cell is composed by a stainless-steel tube and two KBr windows (IR transparent material) separated by a 474 mm distance. The total absorption path through the cell is 948 mm.

A QCL laser head by quality management analysis control system (Q-MACs) is used. The diode employed to measure the CO density is operating in the 2210–2015 cm^{-1} range and is driven in the so-called intra-pulse mode. The laser wavelength is coarsely tuned by the temperature of the laser diode, which is controlled via a Peltier element in contact with the diode. The emission wavelength of the QCL is fine-tuned by the temperature change caused by the current flowing during the pulse. The laser beam coming directly from the diode is collimated with an off-axis parabolic gold mirror (M1) and is then directed by a mirror (M2) through the double-pass cell. The laser beam is focused on an infrared gallium arsenide detector which has a 1 ns response time (IRDM-1GA, neoplascontrol, Q-MACS) via a lens (L). The signal is recorded with a digitizing oscilloscope (LeCroy Waverunner 610zi, 1 GHz). Since mid-IR is not directly visible, the optical alignment is performed with a red laser diode (alignment laser) after overlapping its beam pathway with the IR laser. Data acquisition is performed on a PC and processed using the Q-MACSoft Monitor software [44].

The absorption spectroscopy measurement is based on the Beer–Lambert relation between the incident $I_0(\nu)$ and the transmitted $I(\nu)$ intensities of the laser radiation. For an homogeneous absorption medium the law can be expressed as [45, 46]:

$$\frac{I(\nu)}{I_0\,(\nu)} = \exp\{-k\,(\nu)\,.l\}, \tag{4}$$

where l is the absorption length, which is 948 mm for the present setup and k the absorption coefficient, which is given by

$$k\,(\nu) = n.S.\emptyset\,(\nu) \tag{5}$$

with n (cm^{-3}) the density of the absorbing species, $\emptyset\,(\nu)$ (s) the normalized line profile $\left(\int_{-\infty}^{+\infty} \emptyset\,(\nu)\,.\mathrm{d}\nu = 1\right)$ and S (cm/molecule) the line strength. Integrating equation (4), the number density of the absorbing species is then defined as

$$n = \frac{1}{S.l} \int_{-\infty}^{+\infty} \ln\left(\frac{I_0\,(\nu)}{I\,(\nu)}\right) \mathrm{d}\nu. \tag{6}$$

The CO density is measured using the 2212.625 cm^{-1} absorption line (transition R19) [47]. The line strength at 296 K is 5.546×10^{-20} cm/molecule [47]. The gas temperature of the plasma is probably in the 350–500 K range [27, 34],

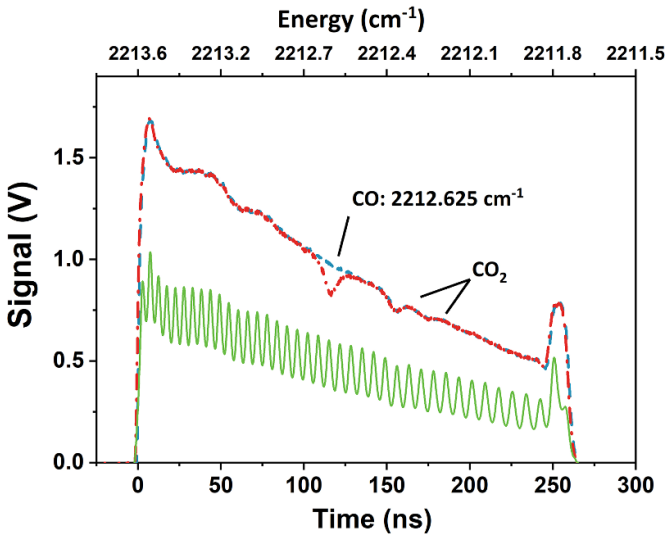

Figure 6. Spectrum of CO at around 2212 cm^{-1} as a function of the scanning time of the QCL (bottom) and its conversion in wavenumbers (top). Dash blue line: signal without any absorption (base line), dash dot red line: signal with absorption and green line: fringes from the Fabry–Perot germanium etalon.

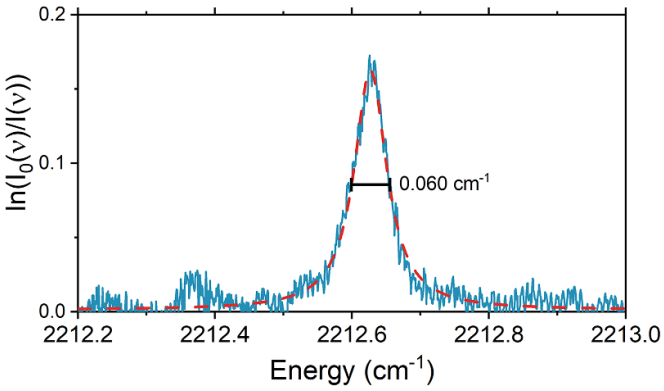

Figure 7. Sample of CO absorption spectrum versus wavelength. Blue line: experimental data and dash red line: fit of the line. Conditions: 400 mbar, 400 sccm CO_2, $V_{pp} = 15$ kV.

but due to the time of flight of the gas to reach the double-pass cell, where the CO concentration is measured, the gas has time to cool down to room temperature. Consequently, we can assume that the gas temperature is close to 296 K. An example of absorption spectra is shown in figure 6. Two CO_2 absorption lines appear in this spectrum range as well, whose relative intensity is weak. As only a small amount of CO_2 is converted into CO, no visible change is observed in these two lines when the plasma was on.

In order to sweep the QCL frequency over the CO absorption line of interest, a 250 ns laser pulse is used, as shown in figure 6. The raw QCL signal without any absorption (dash blue lines) and with absorption (dash dot red line) are recorded as a function of time, which has to be converted into a wavelength scale. This is carried out by recording the fringes of a germanium Fabry–Perot etalon with a known free spectral range of 0.0485 cm^{-1} (green lines). Due to the characteristic response of the QCL to the current pulse, about 10 ns of the laser signal has to be neglected at the beginning and the end of the laser pulse for further analysis. After converting the time scale to a frequency scale, the etalon fringes are used to obtain a relative wavenumber calibration. For the laser diode used here, a non-linear correlation between time and the relative frequency of the frequency-down chirp of the laser was found and fitted with a fifth order polynomial.

According to equation (6) the integrated absorbance, $\int_{-\infty}^{+\infty} \ln\left(\frac{I_0(\nu)}{I(\nu)}\right) d\nu$, has to be evaluated from the spectra to calculate the number density of the absorbing species, n. An example of a CO absorption spectrum is shown in figure 7. The observed CO line (blue line) is fitted by a Lorentzian profile (dash red line) in order to measure the integrated absorbance. We can assume here that the line has a Lorentzian profile since the pressure is high (between 400 and 700 mbar). The number density can then be calculated by dividing the integrated absorbance of a line with the absorption length, l, and the line strength S. The Lorentzian fitting gives a FWHM of approximately 0.060 cm^{-1}.

For each data acquisition, an average of ten samples is measured and the detection limit is evaluated to be 2.10^{20} m^{-3}.

3. Results and discussion

In this section results from electrical characterization, namely filament statistics and their dependence on operational parameters is discussed. This is followed by a section in which the results of the dependence of CO_2 conversion on operational parameters are presented and discussed. Next the results about CO_2 conversion measured with few filaments (<5) is compared with the results from multi filamentary discharges (>100) from the literature. A discussion about the absolute number of CO molecules per filament is also presented which can be used directly to improve the numerical models to understand CO_2 dissociation in DBDs. Later a detailed discussion about energy efficiency in the experiments is presented. Finally, we present the common thread connecting all the experimental results with a discussion about electron kinetics involved in CO_2 filamentary discharges.

3.1. Filaments statistics in pure CO_2 discharges

A typical distribution of average number of filaments per half-cycle (N_{avg}) for different values of injected power (P_{In}) is plotted in figures 8(a) and (b) for 200 mbar and 600 mbar respectively. A similar distribution for a constant P_{In} at 0.15 W but at different flows is plotted in figure 8(c). The bars show distribution of number of half-cycles that have exactly one filament, two filaments, three filaments and so on, in normalized units for figures 8(a) and (b). Normalization is done with respect to total number of cycles measured for that particular operational setting (50–60 cycles are used). The average of these distributions, called N_{avg} gives a representative number of filaments for each plasma condition. From figure 8(a), it can be seen that at a low pressure, meaning 200 mbar, the distribution is sharply peaked for low P_{In} and spreads with increasing P_{In}.

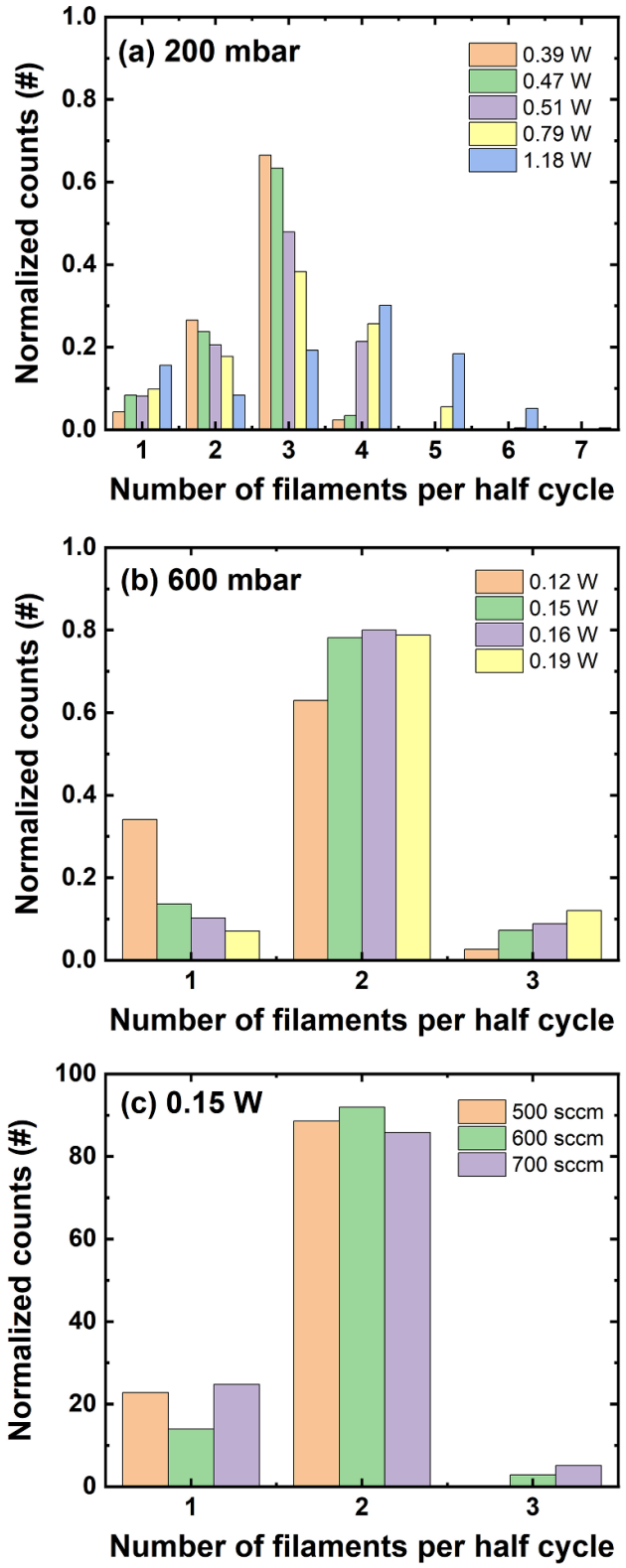

Figure 8. Distributions of number of filaments per half-cycle (N_{avg}) at different injected powers (P_{In}) and constant pressure: (a) at 200 mbar and (b) at 600 mbar. (c) Shows the distribution of filament count with 0.15 W for different flows. Normalization is done with respect to total number of cycles measured for that particular operational setting (50–60 cycles are used).

For example, for the power injection of 1.18 W at 200 mbar the distribution became almost flat (figure 8(a)). Also, as expected with an increase in P_{In}, there is a corresponding increase in the N_{avg}.

Ideally, when every half-cycle is identical, the number of filaments should be the same as a function of the power, and there should be no spread in the distribution even for high P_{In}. However, in a real DBD there are many stochastic processes that will cause broadening of the distribution like we observe in figures 8(a) and (b). For example, Zhang *et al* showed that in a DBD, at certain values of the applied voltage, the number of filaments can vary from one half-cycle to the other [48]. At 200 mbar (figure 8(a)), at low power, the broadening of the distribution decreases, and the chance to get three filaments per half-cycle is more important, while power does not have any effect on the distribution at 600 mbar (figure 8(b)).

From figure 8(c) it becomes immediately clear that the gas flow has no effect on the distribution, which is at first glance surprising, since the renewal of the gas depends on the flow. At low gas flow rate, the residence time of the gas between the two electrodes is expected to be higher than at high gas flow, meaning that an accumulation effect of CO may occur. The gas composition may have an impact on the plasma ignition and its properties (electron density, reduced electric field, temperature, …), and therefore on the CO_2 dissociation and the number of filaments. To estimate the impact of this accumulation effect from a half-cycle to another, we calculated the Péclet number, P_e. This dimensionless number compares the diffusion with the transport of the particles, which is due to the gas flow here. It is defined as:

$$P_e = \frac{UL}{D} \tag{7}$$

where U is the local flow velocity, D, the diffusion coefficient, and, L, the characteristic length, which is in our case the diameter of a filament. Using iCCD pictures we measured the diameter of a filament to be about 150–250 μm (not shown here), which is a typical dimension for this type of filaments [49]. The estimation of the velocity is made from the gas flow rate (in standard conditions), φ, and the cross section of the cell, S, and it is expressed as

$$U = \frac{\varphi\, T\, p_0}{S\, p\, T_0} \tag{8}$$

where p is the pressure in the reactor and p_0 the standard pressure (defined as 1013.25 mbar), T the gas temperature in the cell and T_0 the standard temperature, which is 273 K. The gas temperature in the cell is not homogeneous in the cross section of the cell. For example, the gas temperature in the filament is different from the gas temperature close to the cell windows. As we want to know the flow velocity in the filament, we choose as gas temperature in the cell, T, the temperature of the filament. Thus, we have a top estimate of the flow velocity and the Péclet number as well.

Table 2. Péclet number for various conditions of pressure, flow rate, filament diameter and gas temperature.

	$D = 0.274$ cm^2 s^{-1} $T = 350$ K $p = 700$ mbar		$D = 1.639$ cm^2 s^{-1} $T = 500$ K $p = 200$ mbar	
	$L = 150$ μm	$L = 250$ μm	$L = 150$ μm	$L = 250$ μm
$\phi = 200$ sccm	0.021	0.034	0.017	0.029
$\phi = 700$ sccm	0.072	0.120	0.060	0.100
$\phi = 10\,000$ sccm	1.028	1.714	0.860	1.433

As the electrodes are mounted in the center of a cylindrical cell, S is calculated from the height (6.5 cm) and the width (2.5 cm) of the cell: $S = 16.25$ cm^2. For a gas mixture of CO_2 and CO, the diffusion coefficient is expressed as [50]

$$D\ \left[\text{cm}^2\ \text{s}^{-1}\right] = \frac{1.859 \times 10^{-3} \times T^{\frac{3}{2}} \sqrt{\frac{1}{M_{CO_2}} + \frac{1}{M_{CO}}}}{p\ \sigma^2 \Omega} \qquad (9)$$

where T is the absolute temperature (in K), M the molar mass (in g mol^{-1}), p the pressure (in atm), σ the average collision diameter $(\sigma = \frac{1}{2}(\sigma_{CO_2} + \sigma_{CO}) = \frac{1}{2}(330\ \text{pm} + 376\ \text{pm}) = 353$ pm [51]) and Ω a dimensionless number, usually close to 1. Here we assume $\Omega = 1$. As the molar masses of N_2 and CO are equal, and their kinetic diameters are almost equal (364 pm for N_2 and 376 pm for CO [51]), the diffusion coefficients in CO_2/CO and CO_2/N_2 are very similar. In CO_2/CO, at 288 K and at atmospheric pressure, we calculate a diffusion coefficient of 0.143 cm^2 s^{-1}, which is very close to the one estimated by Wilke and Lee in CO_2 and N_2, who found 0.158 cm^2 s^{-1} [52]. As there is no table of the diffusion coefficient from 200 to 700 mbar for a temperature of 350–500 K range, we use formula (9) for our calculations.

In our case we assume that the absolute temperature in filament is in the range of 350–500 K [27]. The studied pressure is from 200 mbar to 700 mbar, which gives $D = 0.274$ cm^2 s^{-1} at 350 K and 700 mbar and 1.639 cm^2 s^{-1} at 500 K and 200 mbar, which are the two extrema. The Péclet number depends also on the diameter of the filament and the gas flow rate. Table 2 presents its value for various conditions. In our conditions (from 200 to 700 sccm), it varies from 0.017 to 0.120. In any case, this number is lower than 1, and as it is a top estimate, the real value can be even lower. The gas flow effect becomes comparable to the diffusion effect when the Péclet number reaches 1. This condition is met if the gas flow rate rises to 10 000 sccm, which is far from our experimental conditions. Thus, we can conclude that diffusion is more important than the gas flow effects. This is mainly because we look at the movement of particles over a very small distance (150–250 μm). As the diffusion is the main process responsible for particle motion, it explains why there is no gas flow dependence on N_{avg}.

In figure 9, the average number of filaments per half-cycle, N_{avg}, is plotted as a function of P_{In} on a log-log scale for different pressures. N_{avg} is fitted with a straight line as a function of power input. The accuracy of the fit increases if we neglect the conditions when only one filament is present due to an increased accuracy in measuring the power consumed. As said in the electrical characterization section, at low power the area of the Lissajous figure is small, which decreases the accuracy of the absorbed power. The data can be fitted with a power-law with an exponent of 0.3 (the slope of the dotted line on figure 9), which is different from the result of Ozkan *et al*, since they observed a linear dependence of the number of filaments as a function of the power [12]. This difference could be due to the difference in reactor geometry. In addition, as the area of their reactor was bigger, they could not isolate all the filaments and obtain precise values for the number of filaments.

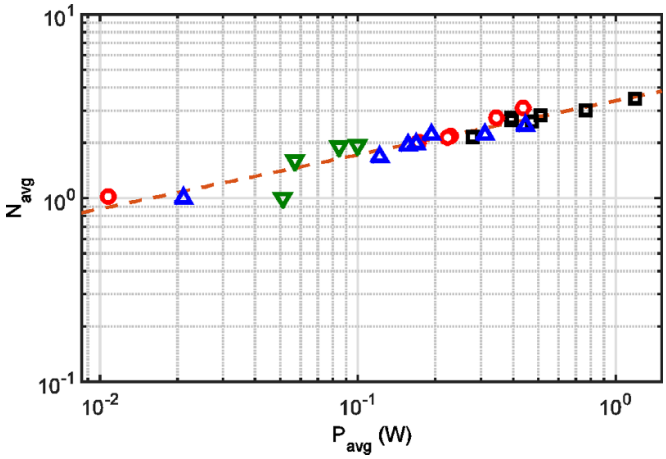

Figure 9. Plot showing the average number of filaments per half-cycle, N_{avg}, as a function P_{In} on a log–log scale; an exponent of 0.3 can be inferred from the fit. Black squares: 200 mbar, red circles: 400 mbar, blue triangles: 600 mbar, green inverted triangles: 800 mbar. The accuracy of the fit increases if we neglect the conditions when only one filament is present due to an increased accuracy in measuring the power consumed.

3.2. CO_2 conversion

3.2.1. Effect of the gas flow rate. Measured CO_2 conversion degrees are displayed as function of the SEI in figure 10. The symbols correspond to different gas flow rates: blue circles for 400 sccm and red squares for 700 sccm. The CO yield increases linearly with the SEI, and varies between 0.004% and 0.06% for SEI between 1 and 80 J l^{-1}.

Taking into account the error margins, one can notice that the conversion degree is independent of the gas flow rate. This

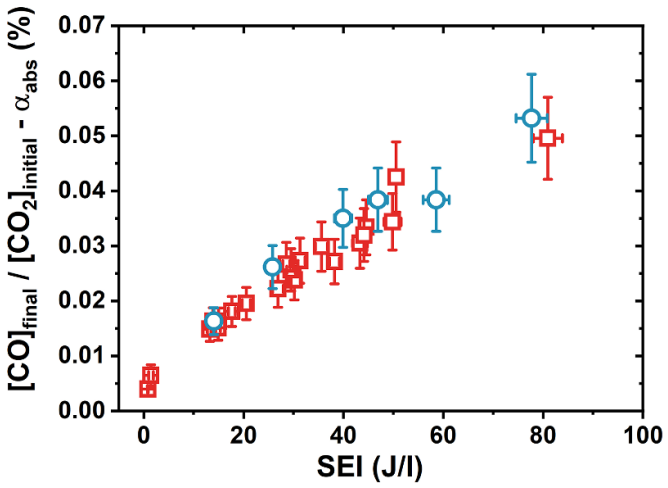

Figure 10. Conversion degree versus the specific energy input at two different gas flows: 400 sccm (blue circles) and 700 sccm (red squares). 400 mbar, pure CO_2.

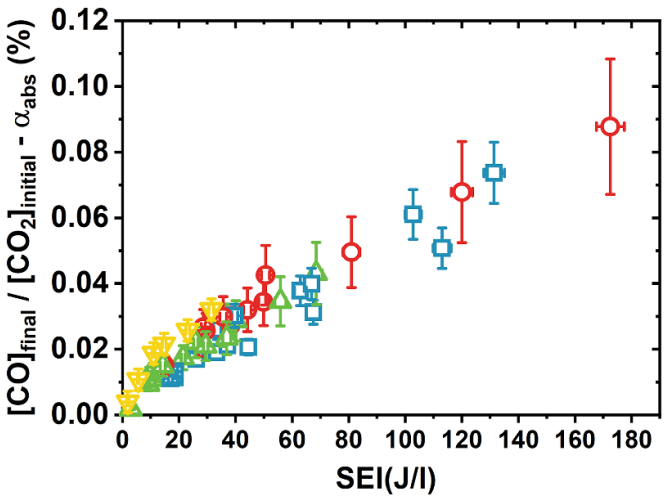

Figure 11. Conversion degree versus the specific energy input at different pressures: 200 mbar (blue square), 400 mbar (red circle), 600 mbar (green up-pointing triangles) and 700 mbar (yellow down-pointing triangles). 700 sccm CO_2.

is due to the fact that the SEI takes into account the flow rate through the reactor and represents the average amount of energy that is spent on each molecule of the gas. If the gas flow changes, the residence time of the gas mixture also changes. These results are in line with what is reported by Brehmer *et al* and explained by fluid modeling by Ponduri *et al* [9, 34]. It should be noted that the lowest conversion degrees are reported for the conditions when N_{avg} is only 1; therefore, a CO_2 conversion degree of approximately 0.005 can be associated per filament.

3.2.2. Effect of the pressure. The effect of pressure on CO_2 conversion is studied by varying pressure in following steps: 200, 400, 600 and 700 mbar with a constant gas flow rate of 700 sccm CO_2. Taking into account the error margins, we observe that the pressure is not the significant variable that effects the CO_2 splitting. As shown in figure 11, the conversion degree does not vary with the pressure, which correlates with the observation that the deposited charge per filament is independent of it as well. This implies that the mean reduced electric field seen by the plasma does not vary and calculations by Hosseini Rad *et al* for an Ar/CO_2 DBD support this interpretation [53].

3.2.3. Comparison with a plane-to-plane reactor. In figures 10 and 11, we notice that the conversion degree increases linearly with the SEI, and varies between 0.004% and 0.10% for SEI between 1 and 170 J l^{-1}. Kozàk *et al* showed using their numerical model that the conversion degree in CO_2 DBDs follows almost a linear law at energies lower than 50 kJ l^{-1}. Previous experiments confirm this linear dependence for energies up to 10 kJ l^{-1}–100 kJ l^{-1} [15, 16, 42].

Table 3 presents the experimental data collected from the literature for CO_2 dissociation in pure CO_2 DBD showing the maximal conversion degree and energy efficiency as a function of the SEI. Most of the works performed on DBDs were done at energies of several tens of kJ l^{-1}, while in the present work the maximum SEI is only 200 J l^{-1} [54]. In order to compare the present results with previous works, we plotted in log–log scale the conversion degree versus SEI in figure 12. The full green circles represent the measures in the pin-to-pin geometry and are the same data of the figure 11. For clarity, we did not make any distinction between the different pressures. Those results are compared with Brehmer's measurements on a CO_2 plane-to-plane DBD at 1000 mbar for different dielectric barrier thicknesses and applied voltage frequencies [9]. The difference between these two geometries affects mainly the number of filaments ignited per unit of time. In order to make the figure clear, the error margins are not shown here, but are in the 10%–20% range.

From figure 12, it can be clearly seen that the CO_2 conversion in a pin-to-pin reactor (green circle) and the plane-to-plane reactor (blue star) follows the same linear trend in log–log scale. A linear trend in log–log scale means a power law and can be expressed as $\alpha = \text{Constant} \times E_{spec}^{n}$, with $n \approx 0.75$, in the 1–10^5 J l^{-1} range. Aerts *et al* showed with their numerical model that the conversion follows a power law as a function of the SEI [42]. For example, they calculated a conversion of almost 10% at 10^5 J l^{-1}, which is similar to the experimental data of Brehmer *et al* (cf figure 12, blue stars). As Aerts *et al* did not plot their results in log–log scale, no direct comparison with the pin-to-pin data is possible. But as the pin-to-pin data (cf figure 12, green dots) follow the same law as the plane-to-plane data (cf figure 12, blue stars), it confirms that for very low energies, i.e. lower than 500 J l^{-1}, the conversion follows also a power law as a function of the SEI. This typical power law can be simplified to a linear law at low value of SEI, which explains the linear law relationship between conversion degree versus the SEI (figures 10 and 11).

In DBDs the energy is not spent homogenously in the gas volume of the discharge, meaning that SEI is at first glance not a good scaling parameter. But our results show that the

Table 3. Experimental data collected from the literature for CO_2 dissociation in pure CO_2 DBD showing the maximal conversion degree and energy efficiency as a function of the specific energy input (SEI). Adapted from Snoeck *et al* [54].

	SEI (J l^{-1})					
Type of DBD	Min	Max	Max conversion degree (%)	Max Energy efficiency (%)	Authors	References
Plan-to-plan	500	50 000	10	5	Brehmer *et al*	[9]
Cylindrical DBD	500	50 000	35	25	Ozkan *et al*	[55]
Cylindrical DBD	5000	200 000	30	15	Belov *et al*	[15]
Cylindrical DBD	5000	500 000	40	8	Aerts *et al*	[42]
Cylindrical DBD	20000	500 000	30	5	Paulussen *et al*	[10]

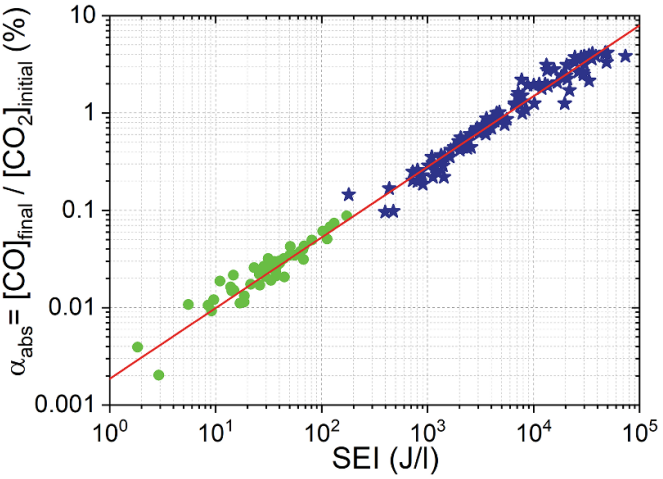

Figure 12. Conversion degree as function of the specific energy input for two types of DBD geometries: pin-to-pin DBD (green circle, data from figure 11) and plan-to-plan DBD (blue star, data from Brehmer *et al* [9]). Reprinted from [9], with the permission of AIP Publishing.

Table 4. Main production processes of CO in a DBD [34].

#	Name of the reaction	Reaction
(R2)	*Electron impact dissociation*	$CO_2 + e^- \rightarrow CO + O + e^-$
(R3)	*Dissociative electron attachment*	$CO_2 + e^- \rightarrow CO + O^-$
(R4)	*Recombination processes*	$CO_2^+ + e^- \rightarrow CO + O$

conversion degree depends on the number of filaments which depends on the SEI, which lead to the conclusion that the SEI, has been shown to be valid as a universal scaling parameter even for DBDs and this is also true at very low SEIs when only one filament occurs.

There are several different classes of mechanisms that can result in CO_2 dissociation in a plasma reactor. Broadly, these can be classified as: (1) electron mediated reactions (2) vibrational up-pumping (3) chemical reactions with active species such as atomic O [56]. The main production processes of CO in a DBD are listed in table 4. Numerical models predicted that in a CO_2 DBD, 80% of the CO production is due to electron impact dissociation (R2), while dissociative electron attachment (R3) and recombination processes (R4) contribute each about 10% [28, 34].

The most efficient process to dissociate CO_2 is by vibrational up-pumping along the asymmetric stretching mode [56]. Aerts *et al* showed that in a DBD configuration this channel is significant if there is an accumulation effect. They showed that if the inter-pulse time exceeds about 10 μs, most of the vibrationally excited CO_2 molecules relax back to the ground state and the dissociation by vibrational up-pumping is insignificant [28]. Additionally Ponduri *et al* showed that the generation of CO mainly takes place during the discharge pulses, meaning, when filaments occur [34].

Each filament has a life time of a couple of hundreds nanoseconds, which is definitively too short for the dissociation by vibrational up-pumping in the same filament [17, 57]. If the CO_2 excited molecules pass a couple of filaments locally in a time frame of 10 μs, then an accumulation effect may occur. In our case, there are from one to a couple of filaments in one half-cycle. The typical time between two filaments in the same half-cycle rises a couple of some μs, meaning that dissociation of CO_2 by vibrational up-pumping is not impossible during the same half-cycle. But from the last filament of one half-cycle to the first filament of the following half-cycle, the time is in the 15–25 μs range, which is higher than 10 μs but in the same order of magnitude. Vibrational up-pumping may happen in our case, but it must not be the main process to dissociate CO_2.

In the gas phase, CO is a very stable molecule if the temperature does not exceed 3000 K [56]. Brehmer *et al* measured in pure CO_2 plane-to-plane DBD that the gas temperature was in the range of 300–500 K [27]. We can assume that the gas temperature in our case was similar, meaning that CO was stable. Additionally, the direct recombination of CO and O to CO_2 is spin forbidden [34]. This means that this recombination occurs very slowly on non-catalytic surfaces, like in our experiment. We also recorded the CO concentration as function of time of flight of the gas through the reactor and observed no influence [34, 58]. So we can assume that loss processes are negligible in the present study. Hence most of the oxygen released from CO_2 dissociation ends up in O_2 or O_3 [9]. However, to increase the energy efficiency of CO_2 conversion process the active O released from CO_2 should be reused.

From the data shown in figure 12, it can be concluded that independent of the type of reactor the data points follow the same trend. Thus, the conversion degree seems to be independent of the geometry of the DBD reactor. This confirms the fact that the SEI in a filamentary DBD determines the density of chemical species produced by an electron impact collision process [34]. Since CO is mainly produced by direct electron

impact, it can be explained why the main parameter to control the CO density is the SEI. Higher energy specific input, higher the number of filaments, higher the CO density is. And since the N_{avg} follows a power law, the CO_2 dissociation also follows a power law. If other chemical processes, like vibrational up-pumping or dissociation of CO_2 by active atomic O, would be important such a universal law could not have been seen.

3.2.4. Absolute amount of CO molecules produced by a single filament. The absolute amount of CO molecules produced by a single filament, N_f, can be estimated from the measurement of the number of filaments per half-cycle and the CO concentration. This parameter is important for comparison with numerical models and to evaluate the conversion degree within one filament.

The concentration of CO molecules can be expressed as follow:

$$[CO] = \frac{2N_f f N_{avg} \tau}{V} \tag{10}$$

where τ is the residence time in the cell, N_{avg} the number of filaments per half-cycle, f, the repetition frequency of the applied voltage and V the volume of the cell. Equation (11) can be simplified by replacing τ by

$$\tau = \frac{V\, T_0\, p}{\varphi\, T\, p_0} \tag{11}$$

where p is the pressure in the reactor and p_0 the standard pressure (defined as 1013.25 mbar), φ the total gas flow rate ($m^3\ s^{-1}$) in standard conditions, T the gas temperature and T_0 the standard temperature, which is 273 K. Thus, N_f can be expressed as follow

$$N_f = \frac{[CO]\ \varphi\ p_0 T}{2 f N_{avg}\, p\, T_0} \tag{12}$$

It is interesting to notice that N_f does not depend on the volume of the cell.

Figure 13 presents the number of CO molecules produced per filament as a function of the SEI at different pressures. The gas temperature has not been measured during the experiments discussed here. However, in previous works it has been determined experimentally and calculated through a numerical model in CO_2 DBD. The gas temperature was found to be in the 350–500 K range [27, 34]. For the data of figure 13, we chose 400 K as a gas temperature. The number of CO molecules produced per filament is in the 5.10^{11}–2.10^{12} range. This number is only weakly dependent on the gas temperature. In any case, these results are in very good agreement with Eliasson's calculations, who calculated from their model that the total number of CO molecules, N_f, formed during a microdischarge, i.e. a filament, in a CO_2 DBD at atmospheric pressure is in the 1.10^{11}–1.10^{12} range [17].

3.2.5. Conversion degree within a filament. The conversion degree within a filament can be deduced from N_f and the number of CO molecules produced per filament. It is expressed as follows:

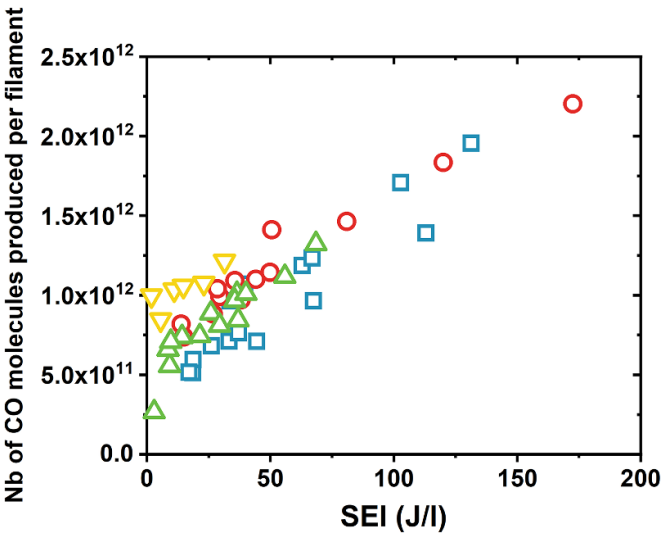

Figure 13. Absolute number of CO molecules produced per filament as a function of the specific energy input at different pressures: 200 mbar (blue square), 400 mbar (red circle), 600 mbar (green up-pointing triangles) and 700 mbar (yellow down-pointing triangles). 700 sccm CO_2. A gas temperature of 400 K is taken.

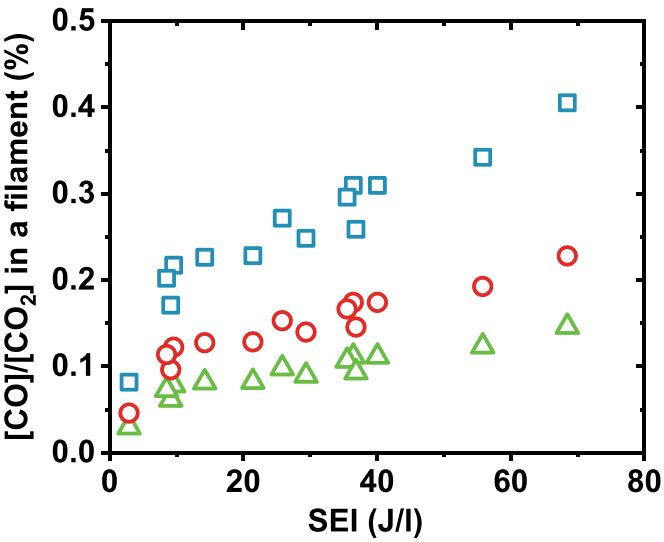

Figure 14. Conversion degree in a filament as a function of the specific energy input at 600 mbar and 700 sccm CO_2. Three different filament diameters are taken: 150 μm (blue square), 200 μm (red circle) and 250 μm (green up-pointing triangles). A gas temperature of 400 K is taken.

$$[CO]\,/\,[CO_2]\,/\text{filament} = \alpha_{\text{filament}} = \frac{N_f\, k_B\, T}{D\pi \left(l/2\right)^2 p} \tag{13}$$

Here, k_B is the Boltzmann constant, T the gas temperature (in K), D the electrode gap (in m), l the filament diameter (in m), and p the pressure (in Pa). The filament diameter is measured to be in the 150–250 μm range. In figure 14 the conversion degree within a filament at 700 sccm CO_2 and 600 mbar is plotted as function of the SEI for different values of filament diameters: 150 μm (blue square), 200 μm (red circle) and 250 μm (green up-pointing triangles). We assume that the

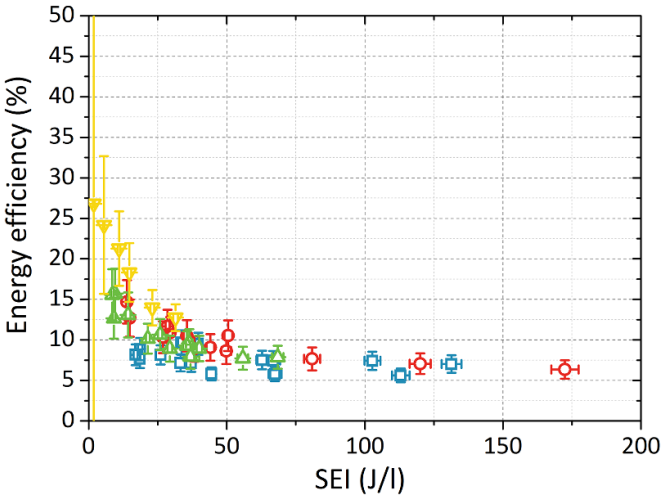

Figure 15. Energy efficiency as a function of the specific energy input at different pressures: blue squares at 200 mbar, red circles at 400 mbar, green up-pointing triangles at 600 mbar and yellow down-pointing triangles at 700 mbar. Conditions: gas flow of 700 sccm CO_2.

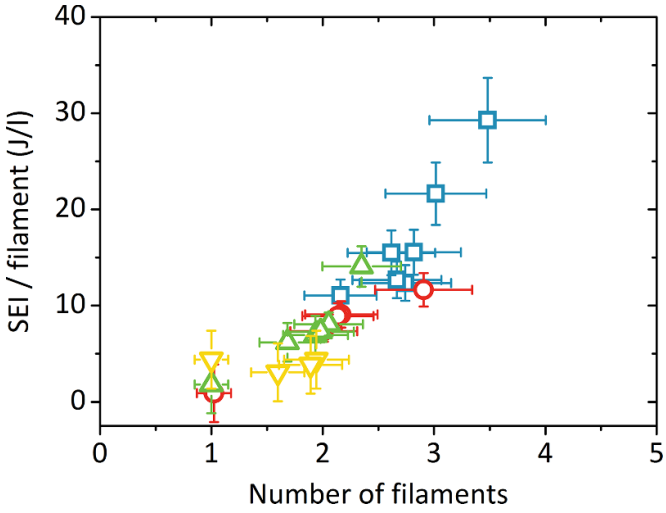

Figure 16. Specific energy input per filament as a function of the number of filaments per half-cycle at different pressures: blue squares at 200 mbar, red circles at 400 mbar, green up-pointing triangles at 600 mbar and yellow down-pointing triangles at 700 mbar. Conditions: gas flow of 700 sccm CO_2.

gas temperature is 400 K. One can notice that the conversion degree is very sensitive to the filament diameter; a four-fold increase in going from 150 μm to 250 μm. In all cases, the conversion degree remains below 1% and increases linearly with the SEI.

3.2.6. Energy efficiency. The current work is mainly focused on the fundamental aspects of CO_2 in a filamentary DBD and hence the energy efficiency of CO_2 conversion is not of prime importance. Nonetheless, we can draw some important conclusions about energy efficiency from a few filaments. The energy efficiency as a function of the SEI at different pressures is presented in figure 15. The CO_2 dissociation is more efficient at lower values of SEI. Taking into account the error margins, it goes up to 25% efficiency. The power law for N_{avg} vs SEI also hints that forming the first filament is easier while subsequent filaments require more energy. Hence, the energy efficiency for CO_2 dissociation also decreases as more energy is spent in creating new filaments. Such trend is not specific to DBDs and is commonly seen in gliding arcs, radio-frequency and microwave discharges as well [8, 59–61]. The maximum of energy efficiency obtained in CO_2 DBDs so far that is reported in literature is around 10% [9, 29, 42], while we report here an energy efficiency of 25%. The main difference in this work compared with previous works lies in the DBD geometry. The dimensions of our DBD are much smaller and only a couple of filaments can occur. In previous works, larger DBDs are used in which several filaments occur.

To understand the power law observed in both N_{avg} (figure 9) and in CO_2 conversion (figure 12) a few observations are outlined here. In figure 16, we show that the energy spent per filament increases with the number of filaments. The first filament chooses the path which requires the less energy (usually the shortest distance). Due to the deposited charges on electrodes, in the same half-cycle, the subsequent filament does not take the same path of the first one, and chooses a path that requires more energy. This energy is even more important due to the presence of deposited charges. This will be the same for the next filaments until the applied voltage is reversed and allow the unloading of the deposited charges. As shown in figure 13, the quantity of CO produced per filament is in the 5.10^{11}–1.10^{12} CO molecules range per filament up to 50 J l^{-1}. The number of filaments increases with the SEI (figure 9) and the energy spent per filament increases with the number for filaments (figure 16). Below 50 J l^{-1} and for a fixed pressure, the quantity of CO produced per filament barely increases (figure 13), meaning that each filament produces comparable amounts of CO even if the energy to produce a filament is bigger. Thus, the efficiency of the CO_2 dissociation decreases with the SEI until 50 J l^{-1}. At higher values the efficiency reaches a plateau of around 5% and this value is comparable with other works for CO_2 DBD [9, 29, 42].

4. Conclusion

In this paper, an experimental investigation of the dissociation of CO_2 in DBD was performed using QCL absorption spectroscopy for the *ex situ* determination of CO number density (i.e. CO_2 conversion degree). The reactor geometry provides the opportunity to accurately control the number of filaments per half cycle and allows to study the impact of one single filament on the CO_2 dissociation. We measured that the charge transferred per the first filament remains constant at 0.5 nC irrespective of pressure. We show that the number of filaments follows a power-law with an exponent of 0.3 as a function of the injected power and that the exponent is independent of the

pressure. The absolute number of CO molecules produced per filament is also measured and found to be in the range between 5.10^{11} and 2.10^{12} molecules. This number increases with the SEI. The conversion degree of CO_2 into CO is estimated to be lower than 0.1% within a single filament and increases with SEI. Due to the presence of only a couple of filaments, the maximum of energy efficiency obtained rises up to 25%.

The conversion degree in pin-to-pin DBD has been compared with a plane-to-plane DBD configuration, and the results show that these two reactor geometries follow the same power law, meaning the reactor geometry is not the most important parameter in CO_2 dissociation in DBD. The SEI, which in turn affects mainly the number of filaments ignited per unit of time, is the main parameter for optimizing the energy efficiency. It is shown that single filaments per half period have the highest energy efficiencies. As in the pin-to-pin DBD only a couple of filaments occur, this result means that the dependence of conversion degree on the SEI can be extended to a single filament. From this observation, we conclude that the SEI can be used as a universal scaling parameter down to very low values.

In large DBD, a CO accumulation can occur and influence the number of CO molecules produced per filament. Adding a small amount of CO gas in the feed gas would allow simulating this accumulation. Future work could be dedicated to the study of this effect.

Data availability statement

The data cannot be made publicly available upon publication because no suitable repository exists for hosting data in this field of study. The data that support the findings of this study are available upon reasonable request from the authors.

Acknowledgments

This project has received funding from the European Union's Seventh Framework Programme for research, technological development and demonstration under grant agreement no.606889 Marie Curie ITN RAPID (Reactive Atmospheric Plasma processIng-eDucation network). All support is gratefully acknowledged.

ORCID iDs

C Douat https://orcid.org/0000-0001-9964-4313
O Guaitella https://orcid.org/0000-0002-6509-6934
E Carbone https://orcid.org/0000-0003-3455-0708
R Engeln https://orcid.org/0000-0002-4687-7436

References

[1] Jiang Z, Xiao T, Kuznetsov V L and Edwards P P 2010 Turning carbon dioxide into fuel *Phil. Trans. R. Soc.* A **368** 3343–64
[2] Carbone E and Douat C 2018 Carbon monoxide in plasma medicine and agriculture: just a foe or a potential friend? *Plasma Med.* **8** 93–120
[3] Douat C, Escot Bocanegra P, Dozias S, Robert É and Motterlini R 2021 Production of carbon monoxide from a He/CO_2 plasma jet as a new strategy for therapeutic applications *Plasma Process. Polym.* **18** 2100069
[4] Guerra V, Silva T, Ogloblina P, Grofulović M, Terraz L, Da Silva M L, Pintassilgo C D, Alves L L and Guaitella O 2017 The case for *in situ* resource utilisation for oxygen production on Mars by non-equilibrium plasmas *Plasma Sour. Sci. Technol.* **26** 11LT01
[5] Horváth G, Skalný J D and Mason N J 2008 FTIR study of decomposition of carbon dioxide in dc corona discharges *J. Phys. D: Appl. Phys.* **41** 225207
[6] Indarto A, Yang D R, Choi J W, Lee H and Song H K 2007 Gliding arc plasma processing of CO_2 conversion *J. Hazard. Mater.* **146** 309–15
[7] Silva T, Britun N, Godfroid T and Snyders R 2014 Optical characterization of a microwave pulsed discharge used for dissociation of CO_2 *Plasma Sources Sci. Technol.* **23** 025009
[8] Spencer L F and Gallimore A D 2012 CO_2 dissociation in an atmospheric pressure plasma/catalyst system: a study of efficiency *Plasma Sources Sci. Technol.* **22** 015019
[9] Brehmer F, Welzel S, Van De Sanden M C M and Engeln R 2014 CO and byproduct formation during CO_2 reduction in dielectric barrier discharges *J. Appl. Phys.* **116** 123303
[10] Paulussen S, Verheyde B, Tu X, De Bie C, Martens T, Petrovic D, Bogaerts A and Sels B 2010 Conversion of carbon dioxide to value-added chemicals in atmospheric pressure dielectric barrier discharges *Plasma Sources Sci. Technol.* **19** 034015
[11] Zheng G, Jiang J, Wu Y, Zhang R and Hou H 2003 The mutual conversion of CO_2 and co in dielectric barrier discharge (DBD) *Plasma Chem. Plasma Process.* **23** 59–68
[12] Ozkan A, Dufour T, Silva T, Britun N, Snyders R, Reniers F and Bogaerts A 2016 DBD in burst mode: solution for more efficient CO_2 conversion? *Plasma Sources Sci. Technol.* **25** 055005
[13] Ray D and Subrahmanyam C 2016 CO_2 decomposition in a packed DBD plasma reactor: influence of packing materials *RSC Adv.* **6** 39492–9
[14] Snoeckx R, Heijkers S, Van Wesenbeeck K, Lenaerts S and Bogaerts A 2016 CO_2 conversion in a dielectric barrier discharge plasma: N_2 in the mix as a helping hand or problematic impurity? *Energy Environ. Sci.* **9** 999–1011
[15] Belov I, Paulussen S and Bogaerts A 2016 Appearance of a conductive carbonaceous coating in a CO_2 dielectric barrier discharge and its influence on the electrical properties and the conversion efficiency *Plasma Sources Sci. Technol.* **25** 015023
[16] Yap D, Tatibouët J and Batiot-Dupeyrat C 2015 Carbon dioxide dissociation to carbon monoxide by non-thermal plasma *J. CO2 Util.* **12** 54–61
[17] Eliasson B, Egli W and Kogelschatz U 1994 Modelling of dielectric barrier discharge chemistry *Pure Appl. Chem.* **66** 1275–86
[18] Kogelschatz U, Eliasson B and Egli W 1999 From ozone generators to flat television screens: history and future potential of dielectric-barrier discharges *Pure Appl. Chem.* **71** 1819–28
[19] Peeters F 2015 The electrical dynamics of dielectric barrier discharges *Technische Universiteit Eindhoven*
[20] Peeters F J J, Yang R and van de Sanden M C M 2015 The relation between the production efficiency of nitrogen atoms and the electrical characteristics of a dielectric barrier discharge *Plasma Sources Sci. Technol.* **24** 045006
[21] Guaitella O, Thevenet F, Guillard C and Rousseau A 2006 Dynamic of the plasma current amplitude in a barrier

discharge: influence of photocatalytic material *J. Phys. D: Appl. Phys.* **39** 2964–72
[22] Vezzu G, Lopez J L, Freilich A and Becker K H 2009 Optimization of large-scale ozone generators *IEEE Trans. Plasma Sci.* **37** 890–6
[23] Brehmer F 2015 Shining light on transient CO_2 plasma (Technical University of Eindhoven)
[24] Klarenaar B L M, Brehmer F, Welzel S, van der Meiden H J, van de Sanden M C M and Engeln R 2015 Note: rotational Raman scattering on CO_2 plasma using a volume Bragg grating as a notch filter *Rev. Sci. Instrum.* **86** 046106
[25] Duan X, Li Y, Ge W and Wang B 2015 Degradation of CO_2 through dielectric barrier discharge microplasma *Greenh. Gases Sci. Technol.* **5** 131–40
[26] Yu Q, Kong M, Liu T, Fei J and Zheng X 2012 Characteristics of the decomposition of CO_2 in a dielectric packed-bed plasma reactor *Plasma Chem. Plasma Process.* **32** 153–63
[27] Brehmer F, Welzel S, Klarenaar B L M, van der Meiden H J, van de Sanden M C M and Engeln R 2015 Gas temperature in transient CO_2 plasma measured by Raman scattering *J. Phys. D: Appl. Phys.* **48** 155201
[28] Aerts R, Martens T and Bogaerts A 2012 Influence of vibrational states on CO_2 splitting by dielectric barrier discharges *J. Phys. Chem.* C **116** 23257–73
[29] Kozák T and Bogaerts A 2014 Splitting of CO_2 by vibrational excitation in non-equilibrium plasmas: a reaction kinetics model *Plasma Sources Sci. Technol.* **23** 045004
[30] Bruggeman P and Brandenburg R 2013 Atmospheric pressure discharge filaments and microplasmas: physics, chemistry and diagnostics *J. Phys. D: Appl. Phys.* **46** 464001
[31] Brandenburg R 2018 Corrigendum: dielectric barrier discharges: progress on plasma sources and on the understanding of regimes and single filaments (2017 *Plasma Sources Sci. Technol.* 26 053001) *Plasma Sources Sci. Technol.* **27** 079501
[32] Höft H, Becker M M, Kettlitz M and Brandenburg R 2022 Upscaling from single- to multi-filament dielectric barrier discharges in pulsed operation *J. Appl. Phys.* **55** 424003
[33] Brandenburg R *et al* 2013 Novel insights into the development of barrier discharges by advanced volume and surface diagnostics *J. Phys. D: Appl. Phys.* **46** 464015
[34] Ponduri S *et al* 2016 Fluid modelling of CO_2 dissociation in a dielectric barrier discharge *J. Appl. Phys.* **119** 093301
[35] Pipa A V, Koskulics J, Brandenburg R and Hoder T 2012 The simplest equivalent circuit of a pulsed dielectric barrier discharge and the determination of the gas gap charge transfer *Rev. Sci. Instrum.* **83** 115112
[36] Manley T C 1943 The electric characteristics of the ozonator discharge *Trans. Electrochem. Soc.* **84** 83
[37] Shao T, Long K, Zhang C, Wang J, Zhang D, Yan P and Zhang S 2009 Electrical characterization of dielectric barrier discharge driven by repetitive nanosecond pulses in atmospheric air *J. Electrost.* **67** 215–21
[38] Williamson J M, Trump D D, Bletzinger P and Ganguly B N 2006 Comparison of high-voltage ac and pulsed operation of a surface dielectric barrier discharge *J. Phys. D: Appl. Phys.* **39** 4400–6
[39] Eliasson B and Kogelschatz U 1991 Modeling and applications of silent discharge plasmas *IEEE Trans. Plasma Sci.* **19** 309–23
[40] Heijkers S, Snoeckx R, Kozák T, Silva T, Godfroid T, Britun N, Snyders R and Bogaerts A 2015 CO_2 conversion in a microwave plasma reactor in the presence of N_2 : elucidating the role of vibrational levels *J. Phys. Chem.* C **119** 12815–28
[41] Lebouvier A, Iwarere S A, D'Argenlieu P, Ramjugernath D and Fulcheri L 2013 Assessment of carbon dioxide dissociation as a new route for syngas production: a comparative review and potential of plasma-based technologies *Energy Fuels* **27** 2712–22
[42] Aerts R, Somers W and Bogaerts A 2015 Carbon dioxide splitting in a dielectric barrier discharge plasma: a combined experimental and computational study *ChemSusChem* **8** 702–16
[43] Douat C, Hübner S, Engeln R and Benedikt J 2016 Production of nitric/nitrous oxide by an atmospheric pressure plasma jet *Plasma Sour. Sci. Technol.* **25** 025027
[44] Neoplas control GmbH Q-MACSoft Monitor *Disponible* (available at: www.neoplas-control.de)
[45] Sadeghi N 2004 6. Molecular spectroscopy techniques applied for processing plasma diagnostics *J. Plasma Fusion Res.* **80** 767–76
[46] Welzel S 2009 New enhanced sensitivity infrared laser spectroscopy techniques applied to reactive plasmas and trace gas detection *PhD Thesis*
[47] Rothman L S *et al* 2009 The HITRAN 2008 molecular spectroscopic database *J. Quant. Spectrosc. Radiat. Transfer* **110** 533–72
[48] Zhang Y T, Wang D Z and Kong M G 2006 Complex dynamic behaviors of nonequilibrium atmospheric dielectric-barrier discharges *J. Appl. Phys.* **100** 063304
[49] Kogelschatz U 2002 Filamentary, patterned, and diffuse barrier discharges *IEEE Trans. Plasma Sci.* **30** 1400–8
[50] Cussler E L 1997 *Diffusion: Mass Transfer in Fluid Systems* (New York: Cambridge University Press)
[51] Matteucci S, Yampolskii Y, Freeman B D and Pinnau I 2006 Transport of gases and vapors in glassy and rubbery polymers *Materials Science of Membranes for Gas and Vapor Separation* vol 598 (Chichester: Wiley) pp 1–47
[52] Wilke C R and Lee C Y 1955 Estimation of diffusion coefficients for gases and vapors *Ind. Eng. Chem.* **47** 1253–7
[53] Hosseini Rad R, Brüser V, Schiorlin M, Schäfer J and Brandenburg R 2023 Enhancement of CO_2 splitting in a coaxial dielectric barrier discharge by pressure increase, packed bed and catalyst addition *Chem. Eng. J.* **456** 141072
[54] Snoeckx R and Bogaerts A 2017 Plasma technology—a novel solution for CO_2 conversion? *Chem. Soc. Rev.* **46** 5805–63
[55] Ozkan A, Bogaerts A and Reniers F 2017 Routes to increase the conversion and the energy efficiency in the splitting of CO_2 by a dielectric barrier discharge *J. Phys. D: Appl. Phys.* **50** 084004
[56] Fridman A 2008 *Plasma Chemistry* vol 14 (Cambridge: Cambridge University Press) pp 9951–9
[57] Corke T C, Enloe C L and Wilkinson S P 2010 Dielectric barrier discharge plasma actuators for flow control* *Annu. Rev. Fluid Mech.* **42** 505–29
[58] Hwang D-Y and Mebel A M 2000 Ab initio study of spin-forbidden unimolecular decomposition of carbon dioxide *Chem. Phys.* **256** 169–76
[59] Spencer L F and Gallimore A D 2011 Efficiency of CO_2 dissociation in a radio-frequency discharge *Plasma Chem. Plasma Process.* **31** 79–89
[60] D'Isa F A, Carbone E A D, Hecimovic A and Fantz U 2020 Performance analysis of a 2.45 GHz microwave plasma torch for CO_2 decomposition in gas swirl configuration *Plasma Sour. Sci. Technol.* **29** 105009
[61] Zhang H, Li L, Li X, Wang W, Yan J and Tu X 2018 Warm plasma activation of CO_2 in a rotating gliding arc discharge reactor *J. CO_2 Util.* **27** 472–9